Brief Report

DOI: 10.5582/bst.2016.01218

The periplasmic sensing domain of *Pseudomonas fluorescens* chemotactic transducer of amino acids type B (CtaB): Cloning, refolding, purification, crystallization, and X-ray crystallographic analysis

Abu Iftiaf Md Salah Ud-Din[1], Anna Roujeinikova[1,2,*]

[1] *Infection and Immunity Program, Monash Biomedicine Discovery Institute and Department of Microbiology, Monash University, Clayton, Victoria, Australia;*
[2] *Department of Biochemistry and Molecular Biology, Monash University, Clayton, Victoria, Australia.*

Summary ***Pseudomonas fluorescens* is a plant growth promoting rhizobacterium that provides nutrients for growth and induces systemic resistance against plant diseases. It has been linked with a number of human diseases including nosocomial infections and bacterial cystitis. Chemotactic motility of *P. fluorescens* towards root exudates plays a crucial role in establishing a symbiotic relationship with host plants. The *P. fluorescens* chemotactic transducer of amino acids type B (CtaB) mediates chemotaxis towards amino acids. As a step towards elucidation of the structural basis of ligand recognition by CtaB, we have produced crystals of its recombinant sensory domain and performed their X-ray diffraction analysis. The periplasmic sensory domain of CtaB has been expressed, purified, and crystallized by the hanging-drop vapor diffusion method using ammonium sulfate as a precipitating agent. A complete data set was collected to 2.2 Å resolution using cryocooling conditions and synchrotron radiation. The crystals belong to space group $P2_12_12_1$, with unit-cell parameters a = 34.5, b = 108.9, c = 134.6 Å. Calculation of the Matthews coefficient and the self-rotation function using this data set suggested that the asymmetric unit contains a protein dimer. Detailed structural analysis of CtaB would be an important step towards understanding the molecular mechanism underpinning the recognition of environmental signals and transmission of the signals to the inside of the cell.**

Keywords: Chemotaxis, receptor, sensing domain, symbiosis

1. Introduction

Pseudomonas fluorescens and other fluorescent Pseudomonads belong to the group of plant growth promoting rhizobacteria (PGPR) that form a symbiotic relationship with host plants (*1,2*). PGPR strains exhibit beneficial effects on plants by fixing nitrogen, producing siderophores and solubilizing essential elements in soil (*1,2*). In addition, they exert indirect beneficial effects by preventing growth or activity of phytopathogens and inducing systemic resistance against plant diseases (*2*). They produce different types of secondary metabolites including fungicides and hydrogen cyanide, which protect roots against pathogens (*3*). Furthermore, some strains of *P. fluorescens* participate in biodegradation of xenobiotic compounds and bioremediation of heavy metals (*3,4*).

P. fluorescens is considered to be an opportunistic pathogen for humans (*5*). It has been linked with a number of human diseases including nosocomial infections and bacterial cystitis. In addition, *P. fluorescens* has been isolated from a large number of respiratory specimens taken from hospital patients,

Released online in J-STAGE as advance publication February 28, 2017.

*Address correspondence to:
Dr. Anna Roujeinikova, Infection and Immunity Program, Monash Biomedicine Discovery Institute Department of Microbiology, Department of Biochemistry and Molecular Biology, Monash University, Clayton, Victoria, Australia.
E-mail: anna.roujeinikova@monash.edu

although its association with pulmonary infections is not well understood (*5*). Furthermore, Sutton CL *et al*. (*5*) reported that more than half of the patients with Crohn's disease develop antibodies against *P. fluorescens*. *P. fluorescens* can also cause blood transfusion-related bacteraemia and catheter-associated bacteraemia amongst the immunosuppressed patients (*6*). Nosocomial outbreaks of bacteraemia due to *P. fluorescens* have been reported (*5*). However, the information on pathogenesis mechanism of *P. fluorescens* is very limited.

Flagella-mediated motility and chemotaxis of *P. fluorescens* towards different nutrients present in root exudates or the rhizosphere play a crucial role in establishing a symbiotic relationship with plants (*2,7-9*). Previous mutagenesis studies demonstrated that chemotaxis is important for the root-tip colonization by *P. fluorescens* (*9-11*). Furthermore, motility and chemotaxis are important virulence factors of many pathogenic bacteria, and it is likely that they play an important role in *P. fluorescens* pathogenesis in humans. The environmental chemical signals are sensed by bacterial membrane-embedded methyl-accepting chemotaxis protein (MCP) receptors (*12*). Upon binding of the signal molecule, MCPs trigger a chemotactic signaling cascade and control bacterial movement towards or away from chemoattractants and repellents, respectively (*12*).

Of the 37 putative MCPs identified in the genome of *P. fluorescens* Pf0-1 to date, ligands are known for only seven. The MCPs termed chemotactic transducers of amino acids (CtaB, CtaB, and CtaC) sense amino acids as attractants (*13*). MCPs Pfl01_3768 and Pfl01_0728 were identified as receptors for L-malate, succinate, and fumarate (*14*). Finally, the chemoreceptor for 2-nitrobenzoate NbaY was shown to be involved in the metabolism of aromatic compounds (*15*).

The periplasmic sensing domain of CtaB has been shown to recognize a broad range of amino acids (16 in total) (*13*). The structural basis of how CtaB recognizes its ligands and transmits the signal across the membrane in response to ligand binding is yet to be determined. Data on bacterial receptors that are structurally and functionally homologous to CtaB is limited. The presence of the conserved consensus motif DXXX(R/K)XWYXXA (*16*) and the Cache (calcium channels and chemotaxis receptors) motif (residues 107-185) (*17*) in the amino acid sequence of CtaB allows us to putatively assign it to the family of receptor proteins with a periplasmic tandem Per-Arnt-Sim (PAS) sensing domain (PTPSD) that recognises amino acids directly. The crystal structures of two different PTPSDs with specificity to amino acids have been recently reported, providing first insights into the structural basis of their ligand specificity. Analysis of PTPSD of *Campylobacter jejuni* Tlp3 in complex with isoleucine (PDB code 4xmr) revealed a strongly hydrophobic pocket accommodating the aliphatic side chain of the ligand, consistent with Tlp3's preference for isoleucine and, likely, other branched amino acids such as valine and leucine (*16*). The crystal structure of PTPSD of *V. cholerae* Mcp37 has been reported in complex with alanine and serine (PDB codes 3c8c and 5ave (*18*)). CtaB PTPSD shares 25 and 29% sequence identity with PTPSDs of Tlp3 and Mcp37, respectively. This protein provides an example of a PTPSD-type receptor with an extremely broad substrate specificity. To elucidate the structural basis of the CtaB's ligand promiscuity, we have initiated X-ray crystallographic studies on recombinant CtaB PTPSD. Here, we report its cloning, refolding, purification and crystallization together with the analysis of the diffraction data.

2. Materials and Methods

2.1. *Cloning and overexpression of CtaB PTPSD as inclusion bodies (IBs)*

The membrane topology and the boundaries the periplasmic sensing domain of CtaB (CtaB PTPSD, residues 32-272) from *P. fluorescens* Pf0-1 (UniProt ID Q3KK38) were predicted by TOPCONS server (*http://topcons.net/*) (*19*) (Figure 1). The sequence encoding CtaB PTPSD was codon optimized for expression in *Escherichia coli*, synthesized and ligated into the pET151/D-TOPO vector (Invitrogen) by Genscript to generate an expression vector that harbors an N-terminal His6 tag followed by a TEV protease cleavage site. The expression vector was introduced into *E. coli* BL21 (DE3) (Novagen) and cells were grown in Luria-Bertani medium supplemented with 50 µg/mL ampicillin to an OD_{600} of 0.6 at 310 K. Overexpression of CtaB PTPSD was induced with 0.5 mM isopropyl-b-D-1-thiogalactopyranoside (Thermo Scientific) and growth was continued for 3.5 h at 210 K. The cells were harvested by centrifugation at 6,000 g for 15 min at 277 K. The cells were resuspended in buffer *A* (10 mM Tris-HCl buffer pH 8.0 and 200 mM NaCl), lyzed by sonication and centrifuged at 10,000 g for 30 min at 277 K. SDS-PAGE gel electrophoresis of clarified supernatant and pellet confirmed that CtaB PTPSD expressed in inclusion bodies (IBs).

2.2. *Solubilization of IBs, protein refolding and purification*

Purification of CtaB PTPSD from IBs was performed following the procedure described earlier with some modifications (*20*). Briefly, IBs were washed two times with buffer *B* (10 mM Tris-HCl pH 8.0, 0.2 mM phenylmethanesulfonyl fluoride (PMSF, Sigma-Aldrich), 1% Triton X-100 (Sigma-Aldrich)) and once in buffer *C* (10 mM Tris-HCl pH 8.0, 0.2 mM PMSF), and centrifuged at 10,000 g for 30 min to purify IBs. The IBs were then solubilized in buffer *D* (10 mM Tris/

HCl pH 8.0, 8 M urea (Amresco), 10 mM dithiothreitol (DTT, Sigma-Aldrich), 0.2 mM PMSF) under gentle stirring for 30 min at 277 K. The protein solution was then clarified by centrifugation at 30,000 g for 30 min at 277 K. Protein concentration was determined using the Bradford assay (*21*). CtaB PTPSD was refolded by diluting 100 mg denatured protein into 250 mL buffer *E* (3 M urea, 10 mM Tris-HCl pH 8.0, 0.4 M L-arginine monohydrochloride) followed by a 48 h incubation at 227 K with continuous mixing. The sample was then dialyzed against 7 L buffer *A* for overnight at 277 K. NaCl and imidazole were then added to the protein solution to final concentrations of 500 and 15 mM, respectively. The protein sample was then loaded onto a 5 mL HiTrap Chelating HP column (GE Healthcare) pre-equilibrated with buffer *F* (10 mM Tris-HCl pH 8.0, 500 mM NaCl, 15 mM imidazole). The column was washed with 20 column volumes of buffer *F* containing 20 mM imidazole to remove unbound proteins, and the protein was eluted with buffer *F* supplemented with 500 mM imidazole. The His_6-tag was removed by overnight incubation with a His_6-TEV protease at 277 K while dialyzing the sample against buffer *G* [50 mM Tris-HCl pH 8.0, 2 mM dithiothreitol, 200 mM NaCl, 1% (*v*/*v*) glycerol]. NaCl and imidazole were then added to the sample to final concentrations of 500 and 15 mM, respectively. The TEV protease and the uncleaved protein were removed on a HiTrap Chelating HP column. The flowthrough was concentrated to 2 mL in an Amicon Ultracel 10 kDa cutoff concentrator and purified further by passing through a Superdex 200 HiLoad 26/60 gel-filtration column (GE Healthcare) equilibrated with buffer *A*. The protein purity was estimated to be greater than 95% by the SDS-PAGE analysis (Figure 2). The oligomeric state of $VfcA^{peri}$ was calculated using a calibration plot of log MW versus the retention volume [$V_{retention}$ (mL) = 549.3 – 73.9 × logMW] available at the EMBL Protein Expression and Purification Core Facility website (*http://www.embl.de/pepcore/pepcore_services/protein_purification/chromatography/hiload26-60_superdex200/index.html*).

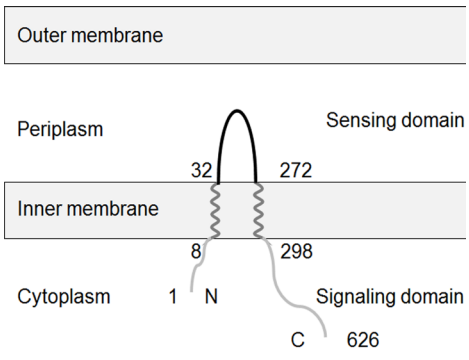

Figure 1. The predicted membrane topology of *P. fluorescens* CtaB and the boundaries of the periplasmic sensory domain CtaB PTPSD characterized in this study.

2.3. *Crystallization*

Prior to crystallization, the protein sample was concentrated to 10 mg/mL, centrifuged for 20 min at 13,000 g and transferred into a clean tube. The preliminary crystallization screening was carried out by the hanging-drop vapour-diffusion method using an automated Phoenix crystallization robot (Art Robbins Instruments). Commercial crystallization screens (Crystal Screen, Index Screen HT, The JCSG Screen and PEG/Ion Screen HT (Hampton Research, Laguna Niguel, CA) were used. Crystals appeared after one day in the condition No. 54 of The JCSG Screen consisting of 0.2 M zinc acetate, 20% (*w*/*v*) polyethylene glycol (PEG) 3000 and 0.1 M imidazole pH 8.0. Refinement to improve the quality of the crystals (Figure 3) resulted in the final optimized condition that contained 14% (*w*/*v*) PEG 3000, 0.15 M zinc acetate sulfate and 0.1 M imidazole pH 7.5.

2.4. *Data collection and processing*

Prior to data collection, crystals were briefly soaked in a cryoprotectant solution consisting of 0.18 M zinc acetate, 20% (*w*/*v*) PEG 3000, 0.1 M imidazole pH 7.5, 10 % (*v*/*v*) glycerol, and cryocooled by plunging in liquid nitrogen. An X-ray diffraction data set was collected from a single crystal on the MX1 beamline of the Australian Synchrotron (AS). A total of 420 images (Figure 4) were collected using a 0.5º oscillation width. The data were processed and scaled using *iMosflm* (*22*) and *AIMLESS* from the *CCP4* suite (*23*). The statistics of data collection and processing are summarized in Table 1.

3. Results and Discussion

Recombinant *P. fluorescens* CtaB PTPSD was expressed

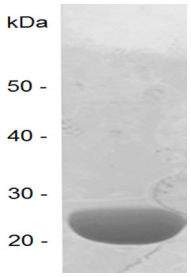

Figure 2. Coomassie Blue-stained 15% SDS-PAGE gel of recombinant CtaB PTPSD.

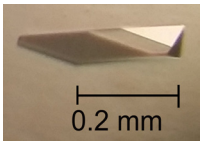

Figure 3. A putative crystal of CtaB PTPSD.

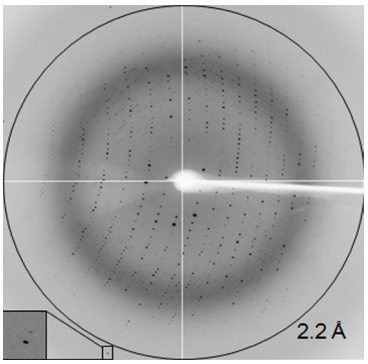

Figure 4. A representative 0.5° oscillation image of the data collected using an ADSC Quantum 210r CCD detector on the MX1 station of the Australian Synchrotron, Victoria, Australia. A magnified rectangle shows diffraction spots beyond 2.2 Å resolution.

Table 1. Data collection and processing

Diffraction source	MX1 beamline, Australian Synchrotron
Wavelength (Å)	1.0
Temperature (K)	100
Detector	ADSC Quantum 210r CCD
Rotation range per image (°)	0.5
Total rotation range (°)	420
Exposure time per image (s)	1
Space group	$P2_12_12_1$
a, *b*, *c* (Å)	34.5, 108.9, 134.6
α, β, γ (°)	90, 90, 90
Mosaicity (°)	0.6
Resolution range (Å)	35.0-2.2 (2.3-2.2)
Total No. of reflections	216,640 (31,679)
No. of unique reflections	26,718 (3,862)
Completeness (%)	100 (100)
Redundancy	8.1 (8.2)
[*I/σ(I)*]	16.2 (4.9)
$R_{pim.}$	0.027 (0.157)
Overall B factor from Wilson plot (Å^2)	41.4

Values for the outer shell are given in parentheses.

with a cleavable N-terminal His6-tag from the pET151/D-TOPO plasmid in *E. coli* BL21 (DE3) upon induction of T7 polymerase. The protein was found in inclusion bodies (IBs). It was refolded from IBs and purified to > 95% electrophoretic homogeneity based on Coomassie Blue staining of SDS-PAGE gels (Figure 2). The protein migrated as a single band on SDS-PAGE with a molecular weight of ~25 kDa. This value was close to molecular weight (26.7 kDa) calculated from the amino acid sequence. When subjected to size-exclusion chromatography, the protein eluted as a single peak with a retention volume of 225 mL corresponding to an approximate molecular weight of 24.5 kDa, which suggested that *P. fluorescens* CtaB PTPSD is a monomer in solution under the tested buffer conditions.

An X-ray diffraction data set was collected from a cryo-cooled crystal of CtaB PTPSD to 2.2 Å using the AS facility (Figure 4). Processing of the diffraction data using the autoindexing routine in *iMosflm* and the analysis of systematic absences implemented in

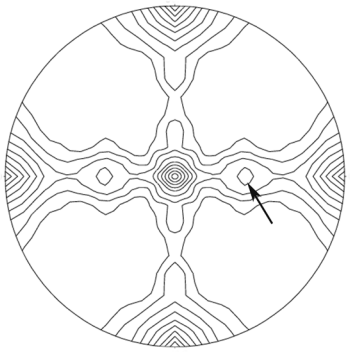

Figure 5. The self-rotation function for CtaB PTPSD (κ = 180°). The noncrystallographic twofold axis is marked by an arrow.

AIMLESS suggested that the crystals have the $P2_12_12_1$ symmetry, with unit cell parameters a = 34.5, b = 108.9, c = 134.6 Å. The average *I/σ(I)* value was 16.2 for all reflections (resolution range 35.0-2.2 Å) and 4.9 in the highest resolution shell (2.3-2.2 Å). A total of 216,640 measurements were made of 26,718 independent reflections. Data processing gave a R_{pim} of 0.027 for intensities (0.157 in the resolution shell 2.3-2.2 Å), and these data were 99.9% complete (100% completeness in the highest resolution shell).

Under the assumption that there are two molecules of CtaB PTPSD in the asymmetric unit, the calculated Matthews coefficient (*24*) was 2.64 Å^3 Da^{-1} and the corresponding solvent content was approximately 53%. Analysis of the self-rotation function computed using *POLARRFN* (*23*) with diffraction data in the resolution range 30-6 Å^3 and an integration radius of 16 Å revealed the presence of a twofold symmetry axis (κ = 180°) represented by a peak at (φ = 44.7°, ω = 0°) with a height of 4σ (Figure 5). Together, this analysis suggests that the CtaB PTPSD crystals contain two molecules per unit cell. Phasing by molecular replacement has not been possible due to low sequence similarity with the known structures deposited in the RCSB PDB database. A search for heavy-atom derivatives with the aim to solve the structure using multiple isomorphous replacement and/or multi-wavelength anomalous dispersion methods is in progress.

We have previously observed that expression of periplasmic sensory domains of bacterial MCP receptors in *E. coli* often results in their deposition predominantly in inclusion bodies (*16,20,25-27*). The recombinant ligand sensing domain of *P. fluorescens* CtaB is another example of a molecule of this type that required extraction from IBs and refolding. We succeeded in producing folded protein and high-quality crystals by following the refolding procedure that we have recently developed (*25,26*). The purified protein was monomeric in solution, in line with previous studies that showed PTPSDs from other receptors to be also monomeric in solution (*16,20,25-27*).

X-ray crystallographic analysis of CtaB PTPSD in complex with various amino acid ligands is expected to provide an explanation of the structural basis behind the broad ligand specificity of this receptor. We note that the crystal structure of PTPSD of another 'promiscuous' amino acid MCP receptor, *V. cholerae* Mcp37, has been recently reported (*18*). However, only the crystal complexes of that protein with alanine and serine have been characterised, which makes it difficult to predict how larger amino acids can fit into its relatively small ligand-binding pocket.

The results presented here are important because they lay the foundation for future systematic structural studies that will be able to address the fundamental biological question of how this receptor, and similar receptors in other important bacteria, sense environmental cues, how they transduce the signal across the membrane and thus control bacterial movement.

Acknowledgements

Part of this research was undertaken on the MX1 beamline of the AS, Victoria, Australia. We thank the AS staff for their assistance with data collection. We are also grateful to Dr. Danuta Maksel and Dr. Robyn Gray at the Monash University Protein Crystallography Unit for assistance with the robotic crystallization trials.

References

1. Glick BR. Plant growth-promoting bacteria: Mechanisms and applications. Scientifica. 2012; 2012:963401.
2. Lugtenberg B, Kamilova F. Plant-growth-promoting rhizobacteria. Annu Rev Microbiol. 2009; 63:541-556.
3. Haas D, Défago G. Biological control of soil-borne pathogens by fluorescent pseudomonads. Nat Rev Microbiol. 2005; 3:307-319.
4. Khan MWA, Ahmad M. Detoxification and bioremediation potential of a *Pseudomonas fluorescens* isolate against the major Indian water pollutants. J Environ Sci Health A Tox Hazard Subst Environ Eng. 2006; 41:659-674.
5. Scales BS, Dickson RP, LiPuma JJ, Huffnagle GB. Microbiology, genomics, and clinical significance of the *Pseudomonas fluorescens* species complex, an unappreciated colonizer of humans. Clin Microbiol Rev. 2014; 27:927-948.
6. Gershman MD, Kennedy DJ, Noble-Wang J, Kim C, Gullion J, Kacica M, Jensen B, Pascoe N, Saiman L, McHale J. Multistate outbreak of *Pseudomonas fluorescens* bloodstream infection after exposure to contaminated heparinized saline flush prepared by a compounding pharmacy. Clin Infect Dis. 2008; 47:1372-1379.
7. Simons M, Permentier HP, de Weger LA, Wijffelman CA, Lugtenberg BJ. Amino acid synthesis is necessary for tomato root colonization by *Pseudomonas fluorescens* strain WCS365. Mol Plant Microbe Interact. 1997; 10:102-106.
8. Kamilova F, Kravchenko LV, Shaposhnikov AI, Azarova T, Makarova N, Lugtenberg B. Organic acids, sugars, and L-tryptophane in exudates of vegetables growing on stonewool and their effects on activities of rhizosphere bacteria. Mol Plant Microbe Interact. 2006; 19:250-256.
9. Muriel C, Jalvo B, Redondo-Nieto M, Rivilla R, Martín M. Chemotactic motility of *Pseudomonas fluorescens* F113 under aerobic and denitrification conditions. PloS One. 2015; 10:e0132242.
10. Singh T, Arora DK. Motility and chemotactic response of *Pseudomonas fluorescens* toward chemoattractants present in the exudate of *Macrophomina phaseolina*. Microbiol Res. 2001; 156:343-351.
11. de Weert S, Vermeiren H, Mulders IH, Kuiper I, Hendrickx N, Bloemberg GV, Vanderleyden J, De Mot R, Lugtenberg BJ. Flagella-driven chemotaxis towards exudate components is an important trait for tomato root colonization by *Pseudomonas fluorescens*. Mol Plant Microbe Interact. 2002; 15:1173-1180.
12. Kato J, Kim H-E, Takiguchi N, Kuroda A, Ohtake H. Pseudomonas aeruginosa as a model microorganism for investigation of chemotactic behaviors in ecosystem. J Biosci Bioeng. 2008; 106:1-7.
13. Oku S, Komatsu A, Tajima T, Nakashimada Y, Kato J. Identification of chemotaxis sensory proteins for amino acids in *Pseudomonas fluorescens* Pf0-1 and their involvement in chemotaxis to tomato root exudate and root colonization. Microbes Environ. 2012; 27:462-469.
14. Oku S, Komatsu A, Nakashimada Y, Tajima T, Kato J. Identification of *Pseudomonas fluorescens* chemotaxis sensory proteins for malate, succinate, and fumarate, and their involvement in root colonization. Microbes Environ. 2014; 29:413-419.
15. Iwaki H, Muraki T, Ishihara S, Hasegawa Y, Rankin KN, Sulea T, Boyd J, Lau PC. Characterization of a pseudomonad 2-nitrobenzoate nitroreductase and its catabolic pathway-associated 2-hydroxylaminobenzoate mutase and a chemoreceptor involved in 2-nitrobenzoate chemotaxis. J Bacteriol. 2007; 189:3502-3514.
16. Liu YC, Machuca MA, Beckham SA, Gunzburg MJ, Roujeinikova A. Structural basis for amino-acid recognition and transmembrane signalling by tandem Per-Arnt-Sim (tandem PAS) chemoreceptor sensory domains. Acta Crystallogr D Biol Crystallogr. 2015; 71:2127-2136.
17. Anantharaman V, Aravind L. The CHASE domain: A predicted ligand-binding module in plant cytokinin receptors and other eukaryotic and bacterial receptors. Trends Biochem Sci. 2001; 26:579-582.
18. Nishiyama S, Takahashi Y, Yamamoto K, Suzuki D, Itoh Y, Sumita K, Uchida Y, Homma M, Imada K, Kawagishi I. Identification of a *Vibrio cholerae* chemoreceptor that senses taurine and amino acids as attractants. Sci Rep. 2016; 6:20866.
19. Tsirigos KD, Peters C, Shu N, Kall L, Elofsson A. The TOPCONS web server for consensus prediction of membrane protein topology and signal peptides. Nucleic Acids Res. 2015; 43:W401-407.
20. Liu YC, Roujeinikova A. Expression, refolding, purification and crystallization of the sensory domain of the TlpC chemoreceptor from *Helicobacter pylori* for structural studies. Protein Expr Purif. 2015; 107:29-34.
21. Bradford MM. A rapid and sensitive method for the quantitation of microgram quantities of protein utilizing the principle of protein-dye binding. Anal Biochem. 1976; 72:248-254.
22. Battye TGG, Kontogiannis L, Johnson O, Powell HR,

Leslie AG. *iMOSFLM*: A new graphical interface for diffraction-image processing with MOSFLM. Acta Crystallogr D Biol Crystallogr. 2011; 67:271-281.
23. Winn MD, Ballard CC, Cowtan KD, Dodson EJ, Emsley P, Evans PR, Keegan RM, Krissinel EB, Leslie AG, McCoy A. Overview of the CCP4 suite and current developments. Acta Crystallogr D Biol Crystallogr. 2011; 67:235-242.
24. Matthews BW. Solvent content of protein crystals. J Mol Biol. 1968; 33:491-497.
25. Machuca MA, Liu YC, Beckham SA, Roujeinikova A. Cloning, refolding, purification and preliminary crystallographic analysis of the sensory domain of the *Campylobacter* chemoreceptor for multiple ligands (CcmL). Acta Crystallogr F Struct Biol Commun. 2015; 71:211-216.
26. Machuca MA, Liu YC, Roujeinikova A. Cloning, expression, refolding, purification and preliminary crystallographic analysis of the sensory domain of the *Campylobacter* chemoreceptor for aspartate A (CcaA). Acta Crystallogr F Struct Biol Commun. 2015; 71:110-113.
27. Machuca MA, Liu YC, Beckham SA, Gunzburg MJ, Roujeinikova A. The crystal structure of the tandem-PAS sensing domain of *Campylobacter jejuni* chemoreceptor Tlp1 suggests indirect mechanism of ligand recognition. J Struct Biol. 2016; 194:205-213.

(Received November 22, 2016; Revised December 20, 2016; Accepted January 16, 2017)